Supporting Online Material for

Real-time Vibrational Dynamics in Chlorophyll a Studied with a Few-Cycle Pulse Laser

1. Methods

1.1 Light source

Supplementary Fig. S1 shows the schematic experimental set-up. We used a noncollinear optical parametric amplifier (NOPA) [1]–[3] as a light source for the pump–probe experiment [4]–[6]. The laser source of this system was a commercial regenerative amplifier (Spitfire; Spectra Physics). Its central wavelength, pulse duration, repetition rate and average output power were 790 nm, 50 fs, 5 kHz and 800mW, respectively. A small fraction of the fundamental was focused on a 1-mm thick sapphire plate to generate white light continuum seed. The main part of the fundamental was used to generate the second harmonic (SH) in a 0.17mm thick BBO (type I), which acted as the pump source of the NOPA after separated from the fundamental. The amplified signal pulse after the double-pass NOPA was first compressed by a pair of chirped mirrors and then a prism pair, resulting in a nearly Fourier transform (FT)-limited 6.8fs pulse with a spectrum extending from 539nm to 738nm, as shown in the inset to Fig. 1.

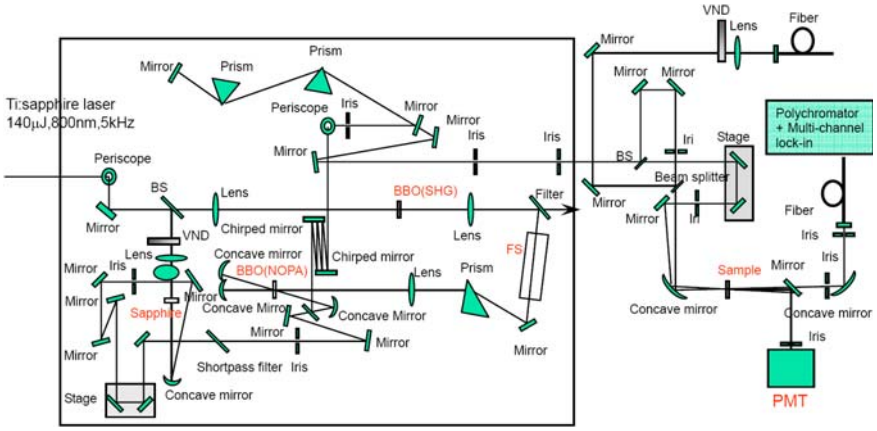

Figure S1. Block diagram of the apparatus of vibration real-time spectroscopy based on a pump-probe scheme. VND: variable neutral-density filter; FS: fused silica; BS: beam splitter.

1.2 Pump-probe spectroscopy

The output beam from the NOPA was divided into two using beam splitter for the pump–probe experiment. In the present study, the pulse energies of the pump and probe were typically about 42 and 6 nJ, respectively. The optical delay of the pump pulse was tuned by a high-resolution, high-precision feedback stage (FS-1020X, Sigma Tech, Inc.). The resolution of each stage step was up to 10 nm, and the

reproducibility accuracy was 20 nm. Both the pump and probe pulses were guided to off-axis parabolic mirrors and focused noncollinearly onto the sample stage with a relative angle of less than 3°. The sample was placed at the focal point of both the pump and probe pulses.

To avoid the problem such as sample damage and heating, in the real-time spectroscopy experiment, we adopted a 0.5 mm flow cell together with the micro annular gear pump (mzr-2905; HNP Mikrosysteme GmbH), which provided a flow rate of 15 ml/min in the present experiment.

We applied the combination of polychromator and multi-channel lock-in amplifier to detect the pump-probe signal. After the sample, the NOPA probe beam was guided to the polychromator by the multimode fiber by an off-axis parabolic mirror, and then dispersed by the polychromator (300 grooves/mm, 500 nm blazed) and guided to the 128 avalanche photodiodes through a 128-channel bundle fiber simultaneously. The spectral resolution of the total system was about 1.5 nm. The wavelength dependent difference absorbance of the probe at 128 wavelengths was measured by changing the pump-probe delay times from -200 to 1800 fs with a 0.8 fs step. All the experiment was performed at a constant temperature (293K).

2. Simulation of the pulse propagation in the sample

Since we used the ultrashort laser pulse in our pump-probe experiment, it was essential to carefully take into account the broadening of the pulse as it propagated through the sample. Using Kramers-Kronig relations, the dependence of the refractive-index change of Chl-*a* on the wavelength could be obtained, as shown in Fig. S2.

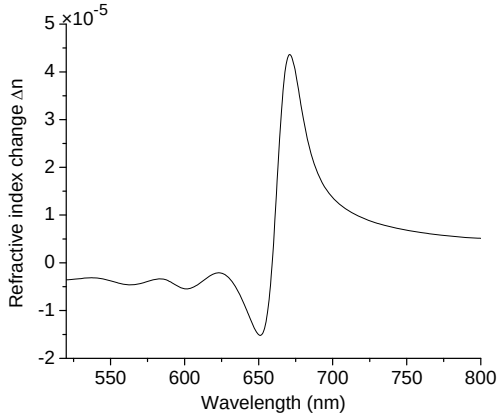

Figure S2. Real refractive index change of Chl-*a*.

Since the refractive index change was very small (~10^{-5}), we could consider the refractive index of Chl-*a* to be constant. Hence, only the effects of the group-velocity dispersion due to the solvent and the loss caused by the stationary absorption of the sample were taken into account in the pulse evolution calculation. First, we measured

the refractive of the solvent as shown in Fig. S3(a), and then we calculated the group-velocity dispersion (GVD) and third-order dispersion (TOD) of the solvent from this data. Using split-step Fourier method, we simulated the pulse propagation from 0 to 1mm with the step of 0.1mm, and the pulse-shape change was plotted in Fig. S3(b) as a function of propagation distance. The spectral change was not shown here, because the laser spectral was only adjusted by the sample absorption effect and it was easy to be obtained. From this calculation, we can see that the pulse has been broadened severely after the propagation of 1 mm solvent. However, for the sample thickness of 0.5mm, the temporal shape only suffered slight change. That is why we used 0.5 mm cell other than 1 mm as used in our previous experiment [7].

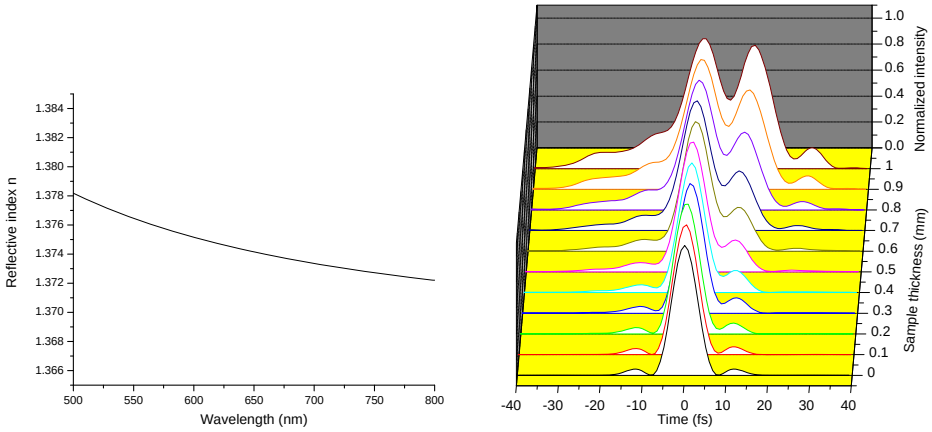

Figure S3. (a) Refractive index of the solvent. (b) The simulation result of temporal change due to the pulse propagation in the sample.

3. Theory appendix

As discussed in the first paragraph of Sec. 3.3, only $|g_0\rangle$ was considered to be the initial state for excitation and only the stimulated process is coupled to the sideband vibrational modes, so we only paid attention to related third-order NL processes depicted by the double-sided Feynman diagrams in Fig. S4, which represented different channels of coherent vibrational excitations in the excited state through the Raman-like process. Here, the pump and probe fields were represented by *Pu* and *Pr*, respectively. ω_0 denoted the Q_y (0-0) emission (central band) or the one with emission energy equal to it. The vibrational bands appearing clearly around the lower energy absorption band, the central band, and the higher energy band in Fig. 3(a) were corresponding to the NL polarizations denoted by $P(\omega_0\text{-}\omega_v)$, $P(\omega_0)$ and $P(\omega_0+\omega_v)$ in Fig. S4, respectively.

Of course there are other four Feynman diagrams describing the NL process due to the excited vibrational coherence besides the above mentioned ones. We did not take them into consideration because the only difference is the sequence of the pump process and all the expressions are the same after excitation. We will concentrate on the former two processes in detail here at first.

For clarity, the two third-order NL processes in Fig. S4(a) described by the

double-sided Feynman diagrams are named as NL process A and B, respectively. Similarly, figures in Fig. S4(b) are describe as the NL processes A′ and B′. The vibrational real-time spectroscopy used in the present experiment is a kind of pump-probe experiment. The signal is equivalent to the response in the broad-band multiplex third-order nonlinear mixing. Because the energy of the probe light is much weaker than that of the pump (typical ratio of 1:7) and we only pay attention to the signal when the pump pulse proceeded the probe pulse by at least 50fs, it can be safely assumed that the pump pulse interacted with the sample twice whereas the probe pulse only once.

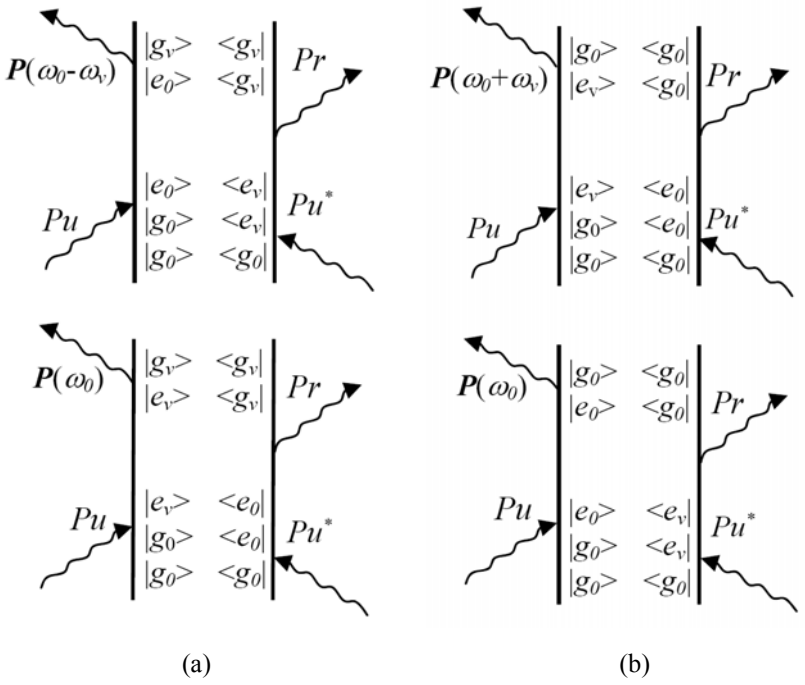

(a) (b)

Figure S4. Double-sided Feynman diagrams of the nonlinear processes related to the stimulated emission. ω_0 is the Qy (0-0) emission frequency (central band) or the one with equal transition energy to it; ω_v represents the vibrational frequency involved in the nonlinear process. The lowest vibrational state in the ground and excited state is represented by g_0 and e_0; g_v and e_v represent where the vibrational coherence exists.

The NL polarization for the NL processes A and B can be calculated and hence the corresponding pump-probe signals. The third-order NL polarizations of the NL processes A and B are given by [8]-[14]

$$\begin{aligned} P_A^{(3)}(t,\tau) = (i/\hbar)^3 \mu^4 \int_0^\infty dt_3 \int_0^\infty dt_2 \int_0^\infty dt_1 E_{pr}(t-t_3) E_{pu}(t-t_3-t_2+\tau) \\ \times E_{pu}^*(t-t_3-t_2-t_1+\tau) \exp\{-i[(\omega_0-\omega_v-\omega')t_3 - \omega_v t_2 \\ -(\omega_0+\omega_v-\omega')t_1 + \omega' t + \theta_{pr}]\} \exp(-t_1/T_2 - t_2/T_{2v} - t_3/T_2) \end{aligned} \quad \text{(S-1)}$$

$$P_B^{(3)}(t,\tau) = (i/\hbar)^3 \mu^4 \int_0^\infty dt_3 \int_0^\infty dt_2 \int_0^\infty dt_1 E_{pr}(t-t_3) E_{pu}(t-t_3-t_2+\tau)$$
$$\times E_{pu}^*(t-t_3-t_2-t_1+\tau) \exp\{-i[(\omega_0-\omega')t_3 + \omega_v t_2 \qquad \text{(S-2)}$$
$$-(\omega_0-\omega')t_1 + \omega' t + \theta_{pr}]\} \exp(-t_1/T_2 - t_2/T_{2v} - t_3/T_2)$$

Here the T_2 and T_{2v} were the electronic dephasing time between $|e\rangle$ and $|g\rangle$ and the vibrational dephasing time between $|e_0\rangle$ and $|e_v\rangle$, respectively. Because the pulse duration in the present experiment is much shorter than the relaxation times, T_2, T_{2v}, and the vibrational period of interest, the envelope functions of the pump and probe electrical fields could be replaced with the δ functions, which highly simplifies the Fourier transforms of Eqs. (S-1) and (S-2). The induced intensity change of the incident probe pulse is proportional to the imaginary part of the NL polarization multiplied by the conjugate of the incident electric field. The observed pump-probe signals, represented by the difference absorption for NL process A and B can be expressed by

$$\Delta A_A(\omega,t) = 2\,\mathrm{Im}[\tilde{E}_{pr}^*(\omega)\tilde{P}^{(3)}(\omega)] / \left|\tilde{E}_{pr}(\omega)\right|^2$$
$$\propto \exp(-\frac{t}{T_{2v}}) \frac{-[\omega-(\omega_0-\omega_v)]\sin(\omega_v t) + \gamma_2 \cos(\omega_v t)}{[\omega-(\omega_0-\omega_v)]^2 + \gamma_2^2} \quad , \qquad \text{(S-3)}$$

$$\Delta A_B(\omega,t) \propto \exp(-\frac{t}{T_{2v}}) \frac{(\omega-\omega_0)\sin(\omega_v t) + \gamma_2 \cos(\omega_v t)}{(\omega-\omega_0)^2 + \gamma_2^2} \quad . \qquad \text{(S-4)}$$

References:

[1] Shirakawa A., I. Sakane, and T. Kobayashi. 1998. Pulse-front-matched optical parametric amplification for sub-10-fs pulse generation tunable in the visible and near infrared. *Opt. Lett.* **23**:1292-1294.

[2] Shirakawa A., I. Sakane, M. Takasaka, and T. Kobayashi. 1999. Sub-5-fs visible pulse generation by pulse-front-matched noncollinear optical parametric amplification. *Appl. Phys. Lett.* **74**: 2268-2270.

[3] Baltuška A., T. Fuji, and T. Kobayashi. 2002. Visible pulse compression to 4 fs by optical parametric amplification and programmable dispersion control. *Opt. Lett.* **27**: 306-308.

[4] Kobayashi T., T. Saito, and H. Ohtani. 2001. Real-time spectroscopy of transition states in bacteriorhodopsin during retinal isomerization, *Nature* **414:** 531-534.

[5] Kobayashi T., A. Shirakawa, H. Matsuzawa, and H. Nakanishi. 2000 Real-time vibrational mode-coupling associated with ultrafast geometrical relaxation in polydiacetylene induced by sub-5-fs pulses. *Chem. Phys. Lett.* **321**: 385-393.

[6] Ishii, N., E. Tokunaga, S. Adachi, T. Kimura, H. Matsuda, and T. Kobayashi. 2004. Optical frequency- and vibrational time-resolved two-dimensional spectroscopy by real-time impulsive resonant coherent Raman scattering in polydiacetylene. *Phys. Rev. A* **70**: 023811.

[7] Wang Y., and T. Kobayashi. 2010. Electronic and vibrational coherence dynamics in a cyanine dye studied using a few-cycle pulsed laser, C*hemPhysChem* **11**: 889-896.

[8] Mukamel, S. 1995. Principles of Nonlinear Optical Spectroscopy. Oxford University Press, New

York.
[9] Parson, W. W. 2007. Modern optical spectroscopy: With Examples from Biophysics and Biochemistry. Springer-Verlag, Berlin.
[10] Mukamel, S. 2000. Multidimensional femtosecond correlation spectroscopies of electronic and vibrational excitations. Annu. *Rev. Phys. Chem.* **51**: 691–729.
[11] Pollard, W. T., S-Y. Lee, and R. A. Mathies. 1990. Wave packet theory of dynamic absorption spectra in femtosecond pump-probe experiments. J. Chem. Phys. 92: 4012-4029.
[12] Walmsley, I. A., and C. L. Tang. 1990. The determination of electronic dephasing rates in time-resolved quantum beat spectroscopy. J. Chem. Phys. 92:1568-1574.
[13] Walmsley, I. A., M. Mitsunaga, and C. L. Tang. 1988. Theory of quantum beats in optical transmission-correlation and pump-probe experiments for a general Raman configuration. Phys. Rev. A 38: 4681-4689.
[14] Mitsunaga, M., and C. L. Tang. 1987. Theory of quantum beats in optical transmission-correlation and pump-probe measurements. Phys. Rev. A 35: 1720-1728.